IEEE Robotics and Automation Letters (RA-L) paper, presented at ICRA 2026, Vienna, Austria. Cite as RA-L paper.

A Phase-Change-Material-Based Variable Stiffness Sheath Inspired by a Multi-Layer Wave Spring Structure for Flexible Upper Gastrointestinal Endoscopic Robots

Dezhi Song, Xiangyu Luo, Xiangyang Yu, Bo Zhang, Zhengbao Yang, *Senior Member, IEEE*, Chengzhi Hu, *Senior Member, IEEE*, and Chaoyang Shi, *Senior Member, IEEE*

***Abstract*—Continuum robots in flexible gastrointestinal endoscopy require transitioning between flexible and rigid states. Phase-change-material-based variable stiffness (VS) methods exhibit a significant stiffness change ratio but are typically time-consuming. These materials are commonly fabricated as simple cylindrical or tubular structures and integrated with continuum joints, overlooking how the VS module's structural characteristics affect stiffness modulation and bending performance. To balance motion flexibility and operational stability, this work presents a stiffness-tunable sheath inspired by a multi-layer wave spring structure, fabricated utilizing thermoplastic material. A water-based active heating/cooling method is employed, wherein the circulation of hot/cold water through silicone tubes helically wrapped around the VS sheath enables rapid thermal regulation. Structural parameters selection of the VS sheath based on the orthogonal design method has been performed to enhance rigid-state stiffness and reduce maximum stress during 90° flexion in a flexible state. Experimental results showed the proposed VS sheath achieves a stiffness change ratio of up to 16.5 times within 30s. After being integrated with a continuum joint, the sheath demonstrates an average positioning error of 1.48 mm within a ±90° bending range in a flexible state, without structural compromise or interference with the continuum joint's bending. In a rigid state, the proposed design can resist 400g external payload with a deflection of less than 6 mm. The efficacy of this design has been validated through ex-vivo experiments on a porcine stomach.**

***Index Terms*—Flexible gastrointestinal endoscopic robot, variable stiffness (VS), phase-change material, continuum joint.**

I. Introduction

CONTINUUM robots have exhibited remarkable capabilities in terms of their compact size, flexible and dexterous movement, and inherent interaction safety, making them highly suitable for navigating through natural orifices or small superficial incisions to perform minimally invasive procedures [1], [2], [3]. Recent developments have seen the creation of several continuum robots to transform treatment methodologies from traditional laparoscopic surgeries to no-scar flexible endoscopic procedures [4], [5]. These emerging techniques require continuum endoscopic arms that can switch between two operational modes: flexible and rigid modes [6], [7]. In the flexible state, the distal continuum joint can execute snake-like movements to navigate complex anatomical pathways without damaging tissues. In the rigid state, the distal continuum joint retains its shape under external forces and provides adequate support when instruments engage with target lesions. Therefore, stiffness regulation in flexible endoscopic continuum robots is crucial, with variable stiffness (VS) approaches categorized into four groups: antagonism mechanism/tension force adjustment [8], [9], jamming [10], [11], [12], shape-locking mechanisms [13], [14], [15] and phase-change materials [16], [17]. Among these methods, phase-change materials such as low-melting-point alloy (LMPA) [18], shape memory alloy (SMA) [19], thermoplastics [20], etc., exhibit significant stiffness changes (up to several dozen times) in response to thermal stimuli through physical property alterations. However, this VS method is typically time-consuming due to the material's prolonged phase transition process [7]. Moreover, current methodologies typically employ the VS module with a simple cylindrical or tubular structure, as either an inside mandrel or outside overtube with the continuum joint, yet overlook the impact of the inherent structural characteristics of the VS module on stiffness modulation and bending motion performance [16], [20], [21]. Consequently, while the flexible endoscopic continuum robot exhibits significant anti-load capabilities in rigid state, it fails to ensure excellent bending performance and positioning accuracy in flexible state.

Received 14 January 2025; accepted 5 May 2025. Date of publication 9 May 2025; date of current version 20 May 2025. This letter was recommended for publication by Associate Editor J. Kim and Editor J. Burgner-Kahrs upon evaluation of the reviewers' comments. This work was supported in part by the National Natural Science Foundation of China under Grant 92148201 and Grant 52475029, and in part by the International Institute for Innovative Design and Intelligent Manufacturing of Tianjin University, Zhejiang, Shaoxing 312000, China. *(Corresponding author: Chaoyang Shi.)*

Dezhi Song, Xiangyu Luo, and Chaoyang Shi are with the Key Laboratory of Mechanism Theory and Equipment Design of Ministry of Education, School of Mechanical Engineering, Tianjin University, Tianjin 300072, China (e-mail: chaoyang.shi@tju.edu.cn).

Xiangyang Yu is with the Department of Gastrointestinal Surgery, Tianjin Hospital of ITCWM/Tianjin Nankai Hospital, Tianjin 300100, China.

Bo Zhang is with Future Robotics Organization, Waseda University, Tokyo 1620044, Japan.

Zhengbao Yang is with the Department of Mechanical and Aerospace Engineering, The Hong Kong University of Science and Technology, Hong Kong SAR 999077, China.

Chengzhi Hu is with the Department of Mechanical and Energy Engineering, Southern University of Science and Technology, Shenzhen 518055, China.

This article has supplementary downloadable material available at https://doi.org/10.1109/LRA.2025.3568564, provided by the authors.

Digital Object Identifier 10.1109/LRA.2025.3568564

IEEE Robotics and Automation Letters (RA-L) paper, presented at ICRA 2026, Vienna, Austria. Cite as RA-L paper.

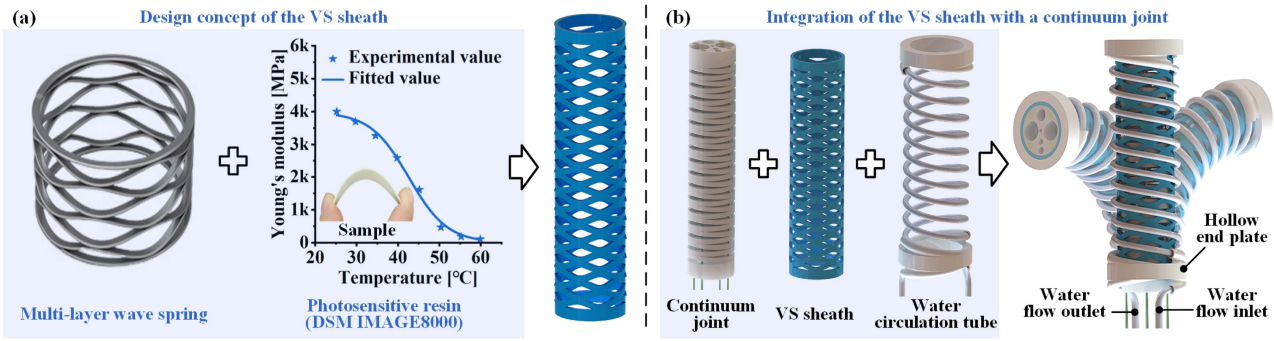

Fig. 1. Structural design of the proposed variable stiffness sheath.

Many attempts have been made to design the VS continuum joint for flexible endoscopic applications. Huu et al. designed a VS endoscopic arm using thermoplastics tubes (Polyethylene Terephthalate, PET) [20]. It realized the transition between the glassy and rubbery states by utilizing electric heating for flexibility and air cooling for rigidity, thus achieving a stiffness change ratio of 22 with a 15s transition time from rigid to flexible state. However, ambient cooling necessitated approximately 100.3s, highlighting the need for active heating and cooling methods to accelerate phase transitions. Zhao et al. developed an LMPA-based VS overtube for the endoscopic arm by exploiting the properties of LMPA that underwent the solid-liquid transition with temperature change [16]. It achieved 18s transitions between states via hot/cold water circulation, though bending performance and positioning accuracy data in its flexible state were lacking. Overall, the state of art focuses on VS mandrel/overtube development using various phase-change materials to enhance the rigid-flexible transition ratio, with active heating/cooling mechanisms proposed to expedite the rigid-flexible transition duration. However, limited attention has been given to VS structure design optimization itself. Yan et al. presented a stiffness-tunable sheath inspired by deep-sea glass sponges, using thermoplastic polymer (thermoplastic starch, TPS) with a 60 °C transition temperature [22]. However, the high phase-change temperature poses thermal injury risks, making it unsuitable for endoscopic surgical applications. Furthermore, hot-melt casting production challenges affect processing quality consistency. Hu et al. proposed an LMPA-based soft VS manipulator inspired by reinforced concrete structures, optimizing the VS layer for rapid stiffness variation with a transition time of 15.7s and rigid state stiffness of 415.45 N/m [23]. However, the VS sheath introduces large positioning errors and motion hysteresis in a flexible state.

To address the aforementioned issues, this work proposes a lightweight, thin-walled variable stiffness sheath inspired by a multi-layer wave spring structure. The VS sheath achieves wide-range and rapid-response stiffness regulation by employing a type of thermoplastic material (photosensitive resin) and an active water-based heating/cooling scheme. Furthermore, this sheath can be readily installed externally on the distal continuum joint of the endoscopic robot, without compromising its original working channel. Structural parameters selection of the VS sheath enhances both its stiffness in a rigid state and the bending performances in a flexible state. The characteristics evaluation and ex-vivo tests are implemented to investigate and validate the proposed VS sheath's performance and effectiveness.

II. Design and Stiffness Analysis

A. Structural Design of the Proposed VS Sheath

The proposed stiffness-tunable sheath features a lightweight, thin-walled tubular design combining high-molecular polymer materials with an active heating/cooling method for stiffness adjustment. The tubular structure is conceptualized and designed based on the inspiration from multi-layer wave spring gaskets, which are renowned for their superior stiffness and torsional resistance characteristics compared to traditional spiral springs [24], [25], as shown in Fig. 1(a). These wave springs are widely used in multi-industrial applications requiring high load capacity and compact dimensions, including automotive shock absorbers, pressure relief valves, and engine vibration isolators [26]. A type of photosensitive resin (DSM IMAGE8000) with a glass transition temperature of approximately 42.6 °C is selected for sheath fabrication, which aligns with the safety standards for surgical procedures [27]. It exhibits temperature-dependent Young's modulus variation, with high stiffness at ambient temperatures (glass state) and low stiffness at elevated conditions (rubber state), as illustrated in Fig. 1(a). This material enables intricate structure formation via stereo lithography apparatus (SLA) processing with 0.2 mm fabrication precision, ensuring consistent quality. Leveraging these advantages, a lightweight VS sheath is developed, as shown in Fig. 1(b). It comprises multiple stacked wave spring units, with an inner diameter (D_{in}) of 16 mm, an outer diameter (D_{out}) of 18 mm, and a total length of 70 mm. This size specification not only complies with the length range (70–180 mm) of the common endoscopic robots' distal continuum bending section but also enables seamless integration with the endoscopic continuum joint developed in our previous work [28], [29]. The designed VS sheath can maintain high stiffness in its rigid state due to the phase-change material being in its glassy state. Conversely, when the material transitions to its rubbery state (with low Young's modulus), the sheath structure exhibits enhanced flexibility without structural compromise or interference with the continuum joint's mobility. The centerline of the single wave spring unit follows as the 3D curve defined by:

$$\begin{cases} x\ (\theta) = R\cos(\theta) \\ y\ (\theta) = R\sin(\theta) \\ z\ (\theta) = A\sin(n\theta) \end{cases}, \tag{1}$$

with $\theta \in [0,\ 2\pi)$. R and A denote the radius of the sheath and amplitude of the wave, respectively. n represents the wave number. The wave spring unit is obtained by sweeping a rectangular

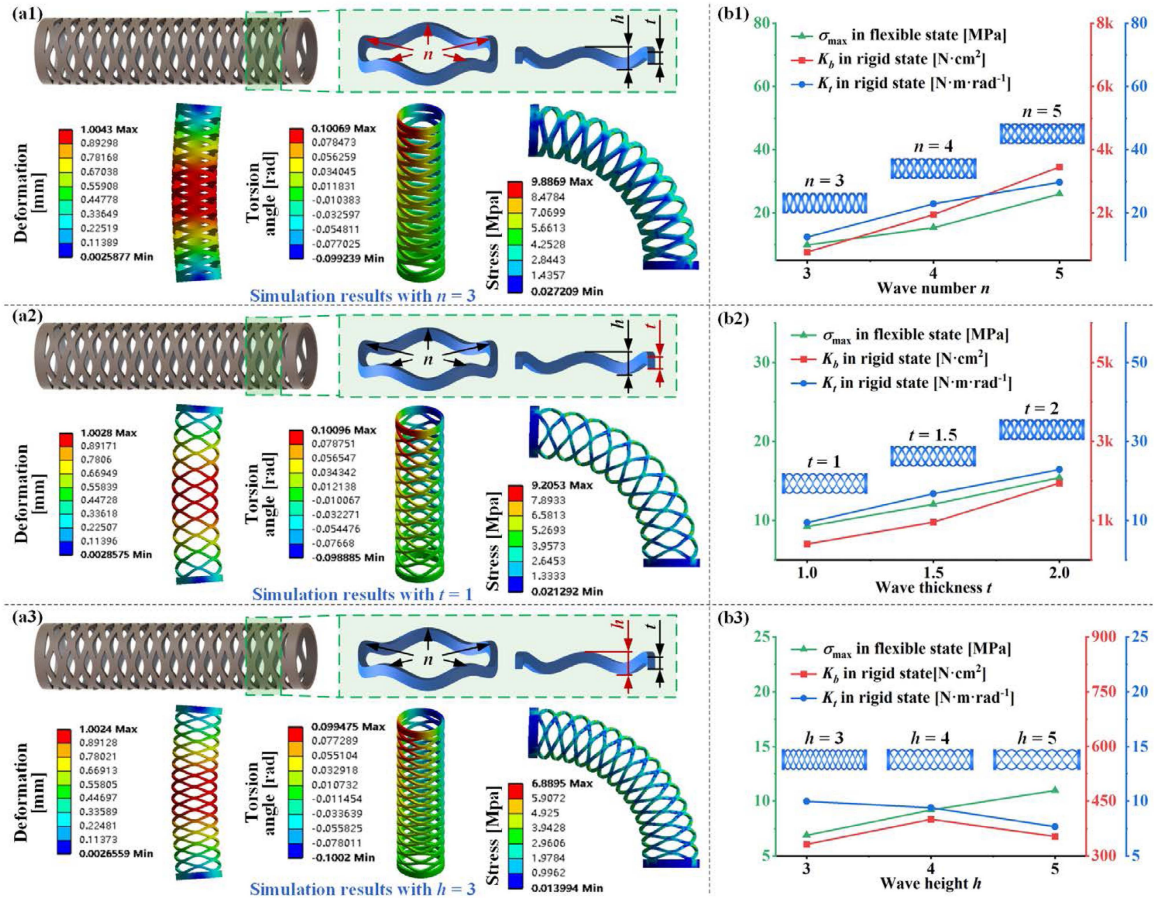

Fig. 2. FEA simulation for evaluating the impact of VS sheath's structural parameters on its stiffness performances: (a1) FEA simulation with varied wave number n (remaining $t = 2$ and $h = 4$) and take $n = 3$ as an example; (a2) FEA simulation with varied wave thickness t (remaining $n = 4$ and $h = 4$) and take $t = 1$ as an example; (a3) FEA simulation with varied wave height h (remaining $n = 4$ and $t = 1$) and take $h = 3$ as an example; (b1) Simulation results with varied wave number n; (b2) Simulation results with varied wave thickness t; (b3) Simulation results with varied wave height h.

cross-section of length $\frac{D_{\text{out}}-D_{\text{in}}}{2}$ and width t along this path. Hence, the wave height h of a single wave spring unit can be calculated as

$$h = 2A + t. \tag{2}$$

A water-based active heating/cooling method is employed to regulate temperature, wherein hot/cold water circulation through silicone tubes facilitates thermal regulation [30]. These silicone tubes are helically wound around the exterior of the VS sheath and securely bonded to the hollow end plate using a sealant (K-946, Kafuter, CN).

B. Analysis of the Impact of Structural Parameters on the Stiffness Performance of the VS Sheath

The bending and torsional stiffness of the designed VS sheath in its rigid state directly impact the loading capacity of the continuum joint. Additionally, the maximum stress experienced when bending to an angle of 90 degrees in its flexible state determines whether structural damage will occur (i.e., when $\sigma_{\max} > [\sigma]$, compromising the VS sheath). To elucidate the impact of VS sheath's structural parameters on these performance metrics, it is crucial to understand the correlation between geometry and stiffness properties. In this context, the structural parameters under consideration include wave number n, wave thickness t, and wave height h of a single wave spring unit. Finite element analysis (FEA) has been conducted using the software ANSYS 18.0 (ANSYS Inc., USA) to evaluate the bending and torsional stiffness in the rigid state, as well as the maximum von Mises stress in the flexible state, as shown in Fig. 2(a1)-(a3). During the FEA simulation, the Young's modulus of the light-cured resin material is temperature-dependent. The corresponding data can be obtained by dynamic mechanical analysis (DMA) tests (supported by Somos Technology Co., Ltd, Changzhou, CN), as graphically represented in Fig. 1(a) and listed in Table I. The bending stiffness K_b is determined by applying a 1 mm displacement at the midpoint of the VS sheath and obtaining the corresponding reaction force, similar to the three-point bending experiment. The torsional stiffness K_t is obtained by applying

TABLE I
THE MATERIAL PROPERTIES FOR FEA SIMULATION

Symbol	Description	Value
E_g	Glassy Young's modulus (rigid state)	3885MPa
E_r	Rubbery Young's modulus (flexible state)	673MPa
ν	Poisson's ratio	0.41

IEEE Robotics and Automation Letters (RA-L) paper, presented at ICRA 2026, Vienna, Austria. Cite as RA-L paper.

TABLE II
ORTHOGONAL TABLE L_9 (3^3) FOR THE STRUCTURAL PARAMETERS SELECTION

No. \ Factor	A (number n)	B (thickness t)	C (height h)
1	1 (3mm)	1 (1.0mm)	1 (3mm)
2	1	2 (1.5mm)	3 (5mm)
3	1	3 (2.0mm)	2 (4mm)
4	2 (4mm)	1	3
5	2	2	2
6	2	3	1
7	3 (5mm)	1	2
8	3	2	1
9	3	3	3

a 1rad angular displacement to the distal end face and recording the resultant reaction torque. The simulation outcomes with different cases are plotted in Fig. 2(b1)-(b3). These results demonstrate that increasing wave number n significantly enhances the bending and torsional stiffness of the VS sheath. The primary factors are the inverse relationship between wave number and the angle formed by the wave relative to the horizontal plane. A more horizontal wave exhibits a lower bending and torsional stiffness. Besides, as n increases, the sheath's maximum stress in its flexible state also rises, potentially inducing structural damage. Wave thickness t similar affects VS sheath stiffness by directly influencing the wave spring unit's cross-sectional moment of inertia. However, the influence of wave height h on performances of the VS sheath exhibits a non-monotonic trend because it affects the number of wave spring units under constant total length. Consequently, excessively large or small values for h will result in a decrease in bending stiffness.

C. Structural Parameters Selection of the VS Sheath Based on Orthogonal Design Method

Based on the analysis presented in the preceding section, selecting the VS sheath's structural parameters aims to maximize both its bending and torsional stiffness in the rigid state while minimizing bending stress in the flexible state. To achieve this, the orthogonal design method is employed to determine the optimal structural parameters of the presented VS sheath in this work, as this approach is well-suited for addressing the multi-factor and multi-index optimization challenges. Three key influencing factors of wave number n, thickness t and height h are selected with each factor set at three levels. An appropriate orthogonal table L_9 (3^3) is subsequently designed for parameter selection, as detailed in Table II. Each configuration of the VS sheath is subjected to FEA simulation, from which the respective bending stiffness K_b, torsional stiffness K_t, and maximum stress $\sigma_{\max}$ values are derived, as summarized in Table III. A comprehensive score is subsequently defined as:

$$\text{Score} = 0.5\frac{\sigma_{\max}}{\max(\sigma_{\max})} - 0.25\frac{K_b}{\max(K_b)} - 0.25\frac{K_t}{\max(K_t)}. \quad (3)$$

This scoring system allows for a balanced assessment of the VS sheath's performance across multiple critical attributes, facilitating the identification of the optimal parameter set that best meets the design objectives. According to the orthogonal analysis, the optimal level combinatorial set of these three factors is A3B2C1 (i.e., $n = 5$, $t = 1.5$, and $h = 3$).

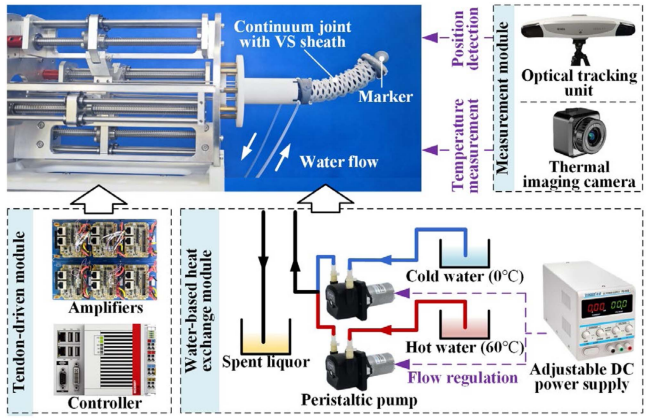

Fig. 3. The experimental setup of the performance's validation for the proposed VS sheath.

III. EXPERIMENTS AND RESULTS

A. Experimental Setup

The experimental configuration encompasses a tendon-actuated module designed for the deflection of the continuum joint and a water-based thermal exchange module intended for stiffness regulation of the proposed VS sheath, as established in Fig. 3. The tendon-driven module consists of an embedded motion controller (CX-5140, Beckhoff, DE) that generates control commands, four amplifiers (Uservo-Flex, MotionG, CN), and four DC servo motors (ECG22SP22, Vishan, Shenzhen, CN) to actuate the ball screws, ensuring precise displacement transmission of the tendons. The thermal exchange module primarily comprises two peristaltic pumps (KPHM600-SV3B17, Kamoer, CN). These pumps circulated hot/cold water, thereby achieving stiffness regulation of the VS sheath. The flow rate of the pumps can be regulated via an adjustable DC power supply.

B. Validation for the Rigid-Flexible Transition Speed of the Proposed VS Sheath

The rigid-flexible transition duration of the proposed VS sheath was validated experimentally at room temperature of approximately 24 °C±1 °C to investigate how water flow rates affect stiffness variation speed. To account for thermal dissipation between the pump and the inlet of the water circulation channel in the presented VS sheath, the hot-water temperature was set to 60 °C, while the cold water was maintained at 0 °C via an ice-water mixture. The surface temperature of the sheath was utilized as a criterion for complete softening/hardening and quantified using an infrared thermal imaging camera (P20M, HIKMICRO, CN) with a resolution of 256 × 192 pixels, as illustrated in Fig. 4(a). Results demonstrated higher flow rates accelerated rigid-flexible transition, as recorded and plotted in Fig. 4(b). Specifically, when the water flow rate was set at 220 mL/min, the VS sheath transitioned from a rigid to a flexible condition within approximately 30 s, while the reverse transition took less than 10s. Active water-based thermal management enabled rigid-flexible transition faster than electric-heating/air-cooling techniques referenced in [22] and [20], ensuring prompt response to surgical emergencies while reducing endoscopist's performance degradation.

TABLE III
SIMULATION RESULTS OF ORTHOGONAL DESIGN

No. \ Factor	A	B	C	K_b [N·cm^2]	K_t [N·m·rad^{-1}]	σ_{max} [MPa]	Score
1	1	1	1	142.9	5.2	5.55	0.0180
2	1	2	3	425.9	8.4	8.00	-0.0043
3	1	3	2	660.3	12.4	9.94	-0.0363
4	2	1	3	311.6	7.7	10.98	0.0572
5	2	2	2	838.9	16.8	12.05	-0.0649
6	2	3	1	1153.3	26.5	14.77	-0.1473
7	3	1	2	620.3	13.3	13.60	0.0130
8	3	2	1	2174.5	24.7	11.36	-0.2807
9	3	3	3	2536.1	25.2	34.13	0.01245
K_1	-0.0226	0.0882	-0.4100				
K_2	-0.1550	-0.3499	-0.0882				
K_3	-0.2552	-0.1711	0.0654				
k_1	-0.0075	0.0294	-0.1367		Optimal level A3 B2 C1		
k_2	-0.0517	-0.1166	-0.0294				
k_3	-0.0851	-0.0570	0.0218				
Range	0.0775	0.1460	0.1585				

K_1, K_2, K_3: The sum of the simulation results at each level of each factor; k_1, k_2, k_3: The average of the simulation results at each level of each factor. Range=max{K_1, K_2, K_3}-min{k_1, k_2, k_3}.

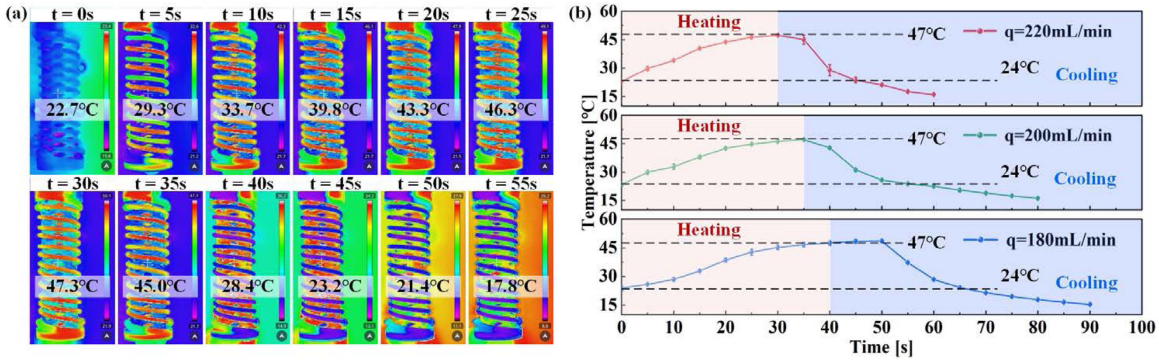

Fig. 4. (a) Temperature distribution obtained by the infrared camera during heating and cooling process (q = 220 mL/min); (b) The experimental results of the VS sheath's surface temperature change with time at different flow rates.

C. Investigation for the Structural Stiffness in Rigid and Flexible States

The structural stiffness of the proposed VS sheath was investigated via standard three-point bending tests using the setup illustrated in Fig. 5(a). The span between the two supporters was adjusted to 70 mm. A commercial force/torque sensor (Nano17, ATI Industrial Automation, USA) was mounted on a ball screw slider, driven downward by DC servo motors at a speed of 0.5 mm/s, capturing real-time force data at a sampling frequency of 60 Hz. The structural stiffness can be determined using the following formula:

$$EI = \frac{FL^3}{48\delta}, \tag{4}$$

where F signifies the loading force, L represents the span, and δ denotes the deflection displacement. Stiffness was assessed in the rigid state (room temperature) and flexible state (after more than 1 minute of hot water circulation). Besides, a separate experiment measured the continuum joint's inherent stiffness without the VS sheath to assess the sheath's impact in its flexible state. The experimental results indicated that the proposed VS sheath significantly increased the stiffness of the continuum joint from 34.30N·cm^2 to 565.95N·cm^2, achieving a rigid-flexible transition ratio of 16.5 times, as plotted in Fig. 5(b). Compared to the case without the VS sheath, the VS sheath in a flexible state caused only a 167% stiffness increase, indicating it maintains sufficient flexibility in its flexible state.

D. Positioning Accuracy Tests of the Continuum Joint With the VS Sheath in the Flexible State

The developed VS sheath was integrated with a continuum joint for ±90° bending tests to evaluate its positioning accuracy in the flexible state (Fig. 6). An optical marker was attached to the distal end of the continuum joint to track its positional changes. Three replicate experiments were conducted in both the horizontal (XZ) and vertical (YZ) bending planes, with results compared to the theoretical values derived from the kinematic model based on the constant curvature assumption, as represented in Fig. 6 and summarized in Table IV. The average positioning error was 1.42 mm in the XZ plane and 1.48 mm in the YZ plane, corresponding to 1.89% and 1.97% of the total length, respectively. The maximum relative position errors in both bending planes did not exceed 5%. Compared with our previous findings [28], integrating the designed VS sheath with the continuum joint hardly resulted in a significant increase in positioning error when the VS sheath was in a flexible state. These experimental results, in conjunction with the results presented in Section III-C, demonstrate that the designed VS

IEEE Robotics and Automation Letters (RA-L) paper, presented at ICRA 2026, Vienna, Austria. Cite as RA-L paper.

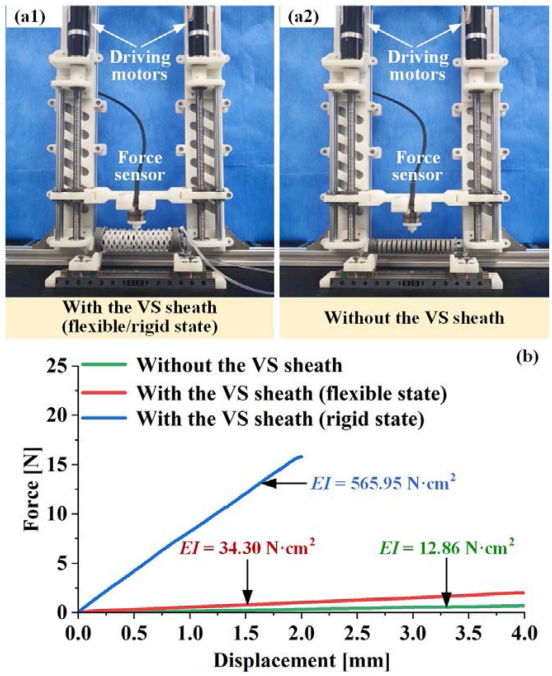

Fig. 5. Structural stiffness tests: (a) The experimental setup: (a1) with the VS sheath; (a2) without the VS sheath; (b) The experimental results.

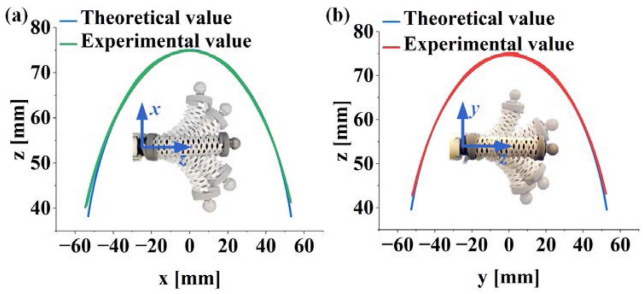

Fig. 6. Positioning accuracy tests in the flexible state: (a) Bending in the XZ plane; (b) Bending in the YZ plane.

TABLE IV
THE POSITIONING ERROR VALUES OF THE PROPOSED VS SHEATH WITH THE CONTINUUM JOINT

	Average value (*)	Maximum value (*)
XZ plane	1.42mm (1.89%)	3.12mm (4.16%)
YZ plane	1.48mm (1.97%)	3.55mm (4.73%)

* Relative error accounting for the total length of the continuum joint.

sheath slightly impacted the bending properties of the continuum joint when it was in a flexible state.

E. Quantification for the Loading Capabilities of the Continuum Joint With the VS Sheath

Standard weights were incrementally loaded at the distal end of the continuum joint in increments of 50g to evaluate the load-bearing capabilities of the continuum joint equipped with the proposed VS sheath in both flexible and rigid states, as shown in Fig. 7. The continuum joint was bent with 45° and 90° in both horizontal and vertical planes and its distal deflection values were measured by the optical tracking unit (Northern Digital Inc, Polaris Vega ST, CA). Each set of experiments was repeated three times, and the weight-displacement relationship was graphically represented in Fig. 7. The experimental results demonstrated that the payload-bearing capacity of the continuum joint in its rigid state was markedly enhanced compared with that in its flexible state. In the rigid state, when subjected to a load of 400g, the deflection remained within 6mm (accounting for 8% of the total length). This finding reveals that the developed VS sheath offers notable enhancements in loading capacity, rendering it apt to manipulate tissue within the GI tract [31].

F. Ex-vivo Test

The VS sheath's efficacy was validated via natural orifice specimen extraction surgery (NOSES) performed on a porcine stomach [32]. The procedure used a flexible endoscopic robot to extract cancerous tissue via the digestive tract, wherein the simulated diseased tissue was pre-positioned within a specimen retrieval bag (more details can be found in the supplementary video). The experimental setup included a dual-armed endoscopic robot with a 400 mm passive bending insertion tube and two manual instrument arms equipped with a snare and forceps, a porcine stomach weighing approximately 500g, and an air compressor to create pneumoperitoneum (Fig. 8(a)). During the ex-vivo experiments, the robot was inserted into the porcine stomach with the VS sheath in a flexible state, as shown in Fig. 8(b1)–(b3), enabling the continuum joint to bend and precisely reach the target position. The VS sheath was then rigidized to stabilize the two instrument arms, thus facilitating the efficient coordination for specimen extraction (Fig. 8(b4)–(b6)). Results show the VS sheath enhances continuum joint stiffness in the rigid state without obstructing instrument channels, enabling complex high-payload operations.

IV. DISCUSSION AND CONCLUSION

This work proposes a phase-change-material-based VS sheath inspired by a multi-wave spring structure, which enables both high loading capability in the rigid state and excellent bending performance in the flexible state. The performance comparison with other types of VS joints can be found in Table V. By employing a water-based active heating/cooling method, the VS sheath accomplishes wide-range and rapid-response stiffness modulation, achieving a stiffness change ratio of up to 16.5 times within 30s. The stiffness adjustment range precisely meets the requirements of standard flexible endoscopes, with a value below 67 N·cm^2 in flexible state and a value above 330 N·cm^2 in rigid state [21]. Compared to [20] and [22], the selected phase change material exhibits a softening temperature of only 42.6 °C, which is lower than the temperature threshold of thermal damage to the human body in the surgical environment, i.e., 45 °C reported in the literature [27]. This ensures operational safety while also reducing the transition duration. Future work will focus on incorporating a heat-insulation sleeve into the outermost layer of the current design to further enhance thermal safety [18].

It is particularly noteworthy that this work selects the structural parameters of the VS sheath. This parameter selection process not only enhances the VS sheath's stiffness in the rigid state but also ensures minimal interference with the bending

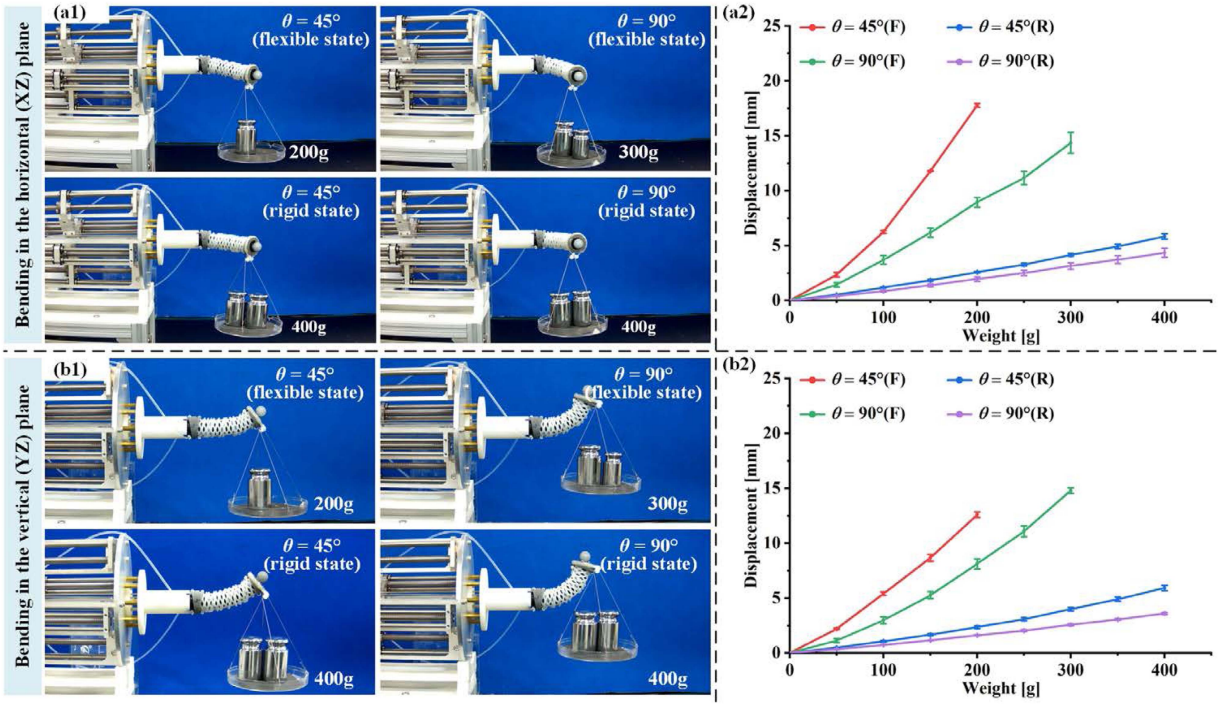

Fig. 7. Loading capacity tests for the VS sheath with a continuum joint in different bending directions. (a1) Loading capacity tests in the XZ bending plane; (a2) Experimental results in the XZ plane; (b1) Loading capacity tests in the YZ bending plane; (b2) Experimental results in the YZ plane.

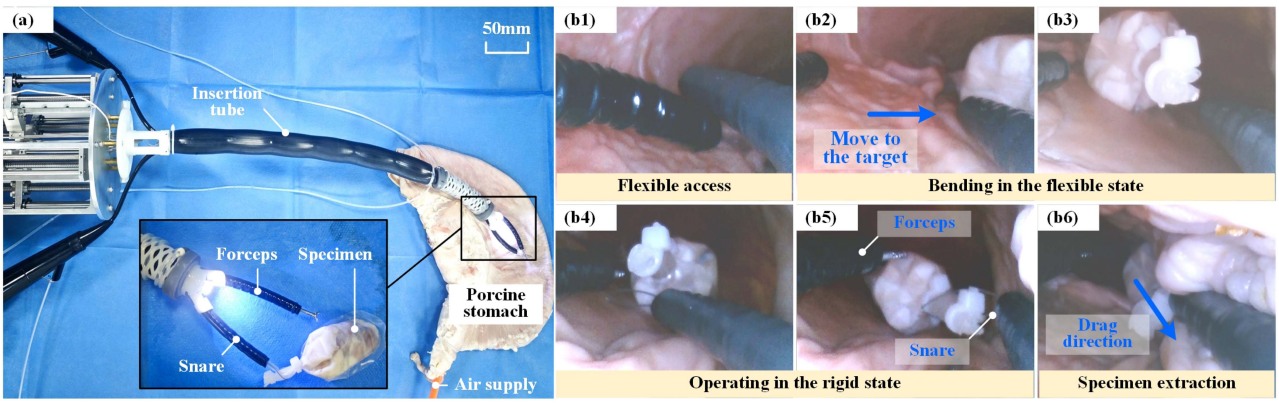

Fig. 8. Ex-vivo test: (a) The experimental setup; (b) Illustration of the specimen extraction procedure.

TABLE V
THE PERFORMANCE COMPARISON OF SEVERAL VS CONTINUUM JOINTS BASED ON DIFFERENT PHASE-CHANGE MATERIALS

Ref.	Material	Phase change tempature [°C]	Thermal stimulation method	Rigid-flexible transition time [s]	Stiffness change ratio	Stiffness [N·cm^2]*	Positioning accuracy in flexible state
[16]	LMPA	47.2	hot/cold water	17 (R→F) 18 (F→R)	≈16.1	≈14124 (R) ≈877 (F)	/
[23]	LMPA	≈49	hot/cold water	15.7 (R→F) 10 (F→R)	/	415.5 (R)	/
[20]	PET	67-70	electric heating and air cooling	30 (R→F) 100.3 (F→R)	22	469.3 (R) 21.3 (F)	/
[22]	TPS	≈60	electric heating and air cooling	28 (R→F) 180 (F→R)	92.3	554 (R) 6 (F)	/
This work	Photosensitive resin	≈42.6	hot/cold water	10 (R→F) 30 (F→R)	16.5	565.9 (R) 34.3 (F)	<1.5mm

* R: rigid state; F: flexible state.

motion of the continuum joint in the flexible state. It achieves an average positioning error of 1.48 mm within a $\pm 90°$ bending range, which is a feature rarely addressed in related works [23]. Despite the distal positioning error showing a slight increase (up to 6.2 mm) after 100 thermal and loading cycles (lasting over 1.5 hours), the VS sheath structure remains intact and exhibits no signs of fatigue damage, demonstrating the design's clinical reliability. The increased error may be attributed to driving tendons creep and slack under prolonged loading conditions. Future work will integrate tension force sensors for real-time tension monitoring and displacement compensation.

The designed sheath can be readily installed externally on the distal continuum joint of the endoscopic robot, without compromising its original working channel. Although this increases the overall outer diameter to some extent (approximately 22 mm, which still meets the requirements of the design specification [33]), this design can retain the advantages of bimanual operation of the dual-armed endoscopic robot compared to placing a VS mandrel inside the continuum joint [20]. Besides, the thin-walled structure developed in this work facilitates its extension to the application on the insertion tube of the endoscopic arm. This is crucial for preventing loop formation in the intestinal tract during interventions performed with the endoscopic surgical robot [34]. Future work will concentrate on developing integrated force and shape sensors for the variable stiffness endoscopic arm, alongside advanced temperature control algorithms, to achieve precise stiffness regulation of the VS sheath [35], [36].

REFERENCES

[1] J. Burgner-Kahrs, D. C. Rucker, and H. Choset, "Continuum robots for medical applications: A survey," *IEEE Trans. Robot.*, vol. 31, no. 6, pp. 1261–1280, Dec. 2015.

[2] P. E. Dupont, N. Simaan, H. Choset, and C. Rucker, "Continuum robots for medical interventions," *Proc. IEEE*, vol. 110, no. 7, pp. 847–870, Jul. 2022.

[3] O. M. Omisore, S. Han, J. Xiong, H. Li, Z. Li, and L. Wang, "A review on flexible robotic systems for minimally invasive surgery," *IEEE Trans. Syst. Man Cybern.-Syst.*, vol. 52, no. 1, pp. 631–644, Jan. 2022.

[4] J. Zhu et al., "Intelligent soft surgical robots for next-generation minimally invasive surgery," *Adv. Intell. Syst.*, vol. 3, no. 5, May 2021, Art. no. 2100011.

[5] J. Kim, M. Mathelin, K. Ikuta, and D.-S. Kwon, "Advancement of flexible robot technologies for endoluminal surgeries," *Proc. IEEE*, vol. 110, no. 7, pp. 909–931, Jul. 2022.

[6] M. Russo et al., "Continuum robots: An overview," *Adv. Intell. Syst.*, vol. 5, no. 5, pp. 2200367, May 2023.

[7] B. Lin, S. Song, and J. Wang, "Variable stiffness methods of flexible robots for minimally invasive surgery: A review," *Biomimetic Intell. Robot.*, vol. 4, no. 3, Sep. 2024, Art. no. 100168.

[8] Y. Kim, S. Cheng, S. Kim, and K. Iagnemma, "A stiffness-adjustable hyperredundant manipulator using a variable neutral-line mechanism for minimally invasive surgery," *IEEE Trans. Robot.*, vol. 30, no. 2, pp. 382–395, Apr. 2014.

[9] H. Kim et al., "Sigmoidal auxiliary tendon-driven mechanism reinforcing structural stiffness of hyper-redundant manipulator for endoscopic surgery," *Soft Robot*, vol. 10, no. 2, pp. 234–245, Apr. 2023.

[10] Y. Kim, S. Cheng, S. Kim, and K. Iagnemma, "A novel layer jamming mechanism with tunable stiffness capability for minimally invasive surgery," *IEEE Trans. Robot.*, vol. 29, no. 4, pp. 1031–1042, Aug. 2013.

[11] E. Amanov et al., "Toward a flexible variable stiffness endoport for single-site partial nephrectomy," *Ann. Biomed. Eng.*, vol. 46, no. 10, pp. 1498–1510, Oct. 2018.

[12] X. Luo et al., "A novel distal hybrid pneumatic/cable-driven continuum joint with variable stiffness capacity for flexible gastrointestinal endoscopy," *Adv. Intell. Syst.*, vol. 5, no. 6, Jun. 2023, Art. no. 2200403.

[13] D. Chung, J. Kim, D. Baek, and D.-S. Kwon, "Shape-locking mechanism of flexible joint using mechanical latch with electromagnetic force," *IEEE Robot. Autom. Lett.*, vol. 4, no. 3, pp. 2661–2668, Jul. 2019.

[14] C. Bishop, M. Russo, X. Dong, and D. Axinte, "A novel underactuated continuum robot with shape memory alloy clutches," *IEEE-ASME Trans. Mechatron.*, vol. 27, no. 6, pp. 5339–5350, Dec. 2022.

[15] B. Lin, J. Wang, S. Song, B. Li, and M. Q.-H. Meng, "A modular lockable mechanism for tendon-driven robots: Design, modeling and characterization," *IEEE Robot. Autom. Lett.*, vol. 7, no. 2, pp. 2023–2030, Apr. 2022.

[16] R. Zhao, Y. Yao, and Y. Luo, "Development of a variable stiffness over tube based on low-melting-point-alloy for endoscopic surgery," *J. Med. Devices*, vol. 10, no. 2, pp. 021002, Jun. 2016.

[17] Q. Le et al., "Development of a variable stiffness modulating mechanism based on phase-change material and a temperature control system," *Int. J. Precis. Eng. Manuf.*, vol. 23, no. 5, pp. 517–531, May 2022.

[18] H. Wang, Z. Chen, and S. Zuo, "Flexible manipulator with low-melting-point alloy actuation and variable stiffness," *Soft Robot.*, vol. 9, no. 3, pp. 577–590, Jun. 2022.

[19] S. Jiang et al., "A variable-stiffness continuum manipulators by an SMA-based sheath in minimally invasive surgery," *Int. J. Med. Robot. Comput. Assist. Surg.*, vol. 16, no. 2, Apr. 2020, Art. no. e2081.

[20] H. Le et al., "A temperature-dependent, variable-stiffness endoscopic robotic manipulator with active heating and cooling," *Ann. Biomed. Eng.*, vol. 48, no. 6, pp. 1837–1849, Jun. 2020.

[21] A. J. Loeve et al., "Polymer rigidity control for endoscopic shaft-guide 'Plastolock' - A feasibility study," *J. Med. Devices*, vol. 4, no. 4, Dec. 2010, Art. no. 045001.

[22] J. Yan et al., "A wide-range stiffness-tunable soft actuator inspired by deep-sea glass sponges," *Soft Robot*, vol. 9, no. 3, pp. 625–637, Jun. 2022.

[23] C. Hu et al., "A miniaturized variable stiffness soft manipulator with a customizable LMPA pattern," *IEEE Robot. Autom. Lett.*, vol. 8, no. 9, pp. 5704–5711, Sep. 2023.

[24] H. R. Erfanian-Naziftoosi, S. S. Shams, and R. Elhajjar, "Composite wave springs: Theory and design," *Mater. Des.*, vol. 95, pp. 48–53, 2016.

[25] Smalley, "Wave spring vs. coil spring," 2024. Accessed: Jan. 2025. [Online]. Available: https://www.smalley.com/blog/wave-spring-vs-coil-spring

[26] M. R. U. Haq et al., "WSdesign: A mathematical design method for generating uniform and functionally gradient/hybrid wave springs, fabricated using additive manufacturing processes," *Int. J. Adv. Manuf. Technol.*, vol. 121, no. 11-12, pp. 7763–7778, 2022.

[27] P. S. Yarmolenko et al., "Thresholds for thermal damage to normal tissues: An update," *Int. J. Hyperthermia*, vol. 27, no. 4, pp. 320–343, May 2011.

[28] D. Song, S. Wang, Z. Zhang, X. Yu, and C. Shi, "A novel continuum overtube with improved triangulation for flexible robotic endoscopy," *IEEE Trans. Med. Robot. Bionics*, vol. 5, no. 3, pp. 657–668, Aug. 2023.

[29] Y. Xu et al., "A novel extensible continuum robot with growing motion capability inspired by plant growth for path-following in transoral laryngeal surgery," *Soft Robot*, vol. 11, no. 1, pp. 171–182, Feb. 2024.

[30] Z. Xing, F. Wang, Y. Ji, D. McCoul, X. Wang, and J. Zhao, "A structure for fast stiffness-variation and omnidirectional-steering continuum manipulator," *IEEE Robot. Autom. Lett.*, vol. 6, no. 2, pp. 755–762, Apr. 2021.

[31] D. Song, X. Yu, B. Leng, B. Zhang, and C. Shi, "Development of a miniature 5-DOF modularized flexible instrument with distal rotation capability for dual-armed upper gastrointestinal endoscopic robots," *IEEE-ASME Trans. Mechatron.*, to be published, doi: 10.1109/TMECH.2025.3563471.

[32] J. Li et al., "A specimen extraction instrument based on braided fiber tube for natural orifice translumenal endoscopic surgery," *J. Med. Devices*, vol. 12, no. 3, pp. 031008, Sep. 2018.

[33] M. Hwang and D. S. Kwon, "K-FLEX: A flexible robotic platform for scar-free endoscopic surgery," *Int. J. Med. Robot. Comput. Assist. Surg.*, vol. 16, no. 2, 2020.

[34] T. Liang, C. Zhang, Y. Wang, S. Zuo, S. Wang, and K. Kong, "A novel robot platform with decoupled stiffness control for endoscopic surgery," *IEEE Robot. Autom. Lett.*, vol. 9, no. 10, pp. 8635–8642, Oct. 2024.

[35] Y. Hao, H. Zhang, Z. Zhang, C. Hu, and C. Shi, "Development of force sensing techniques for robot-assisted laparoscopic surgery: A review," *IEEE Trans. Med. Robot. Bionics*, vol. 6, no. 3, pp. 868–887, Aug. 2024.

[36] C. Shi et al., "Shape sensing techniques for continuum robots in minimally invasive surgery: A survey," *IEEE Trans. Biomed. Eng.*, vol. 64, no. 8, pp. 1665–1678, Aug. 2017.